Supplementary material - Physical constraints for effective magma-water interaction along volcanic conduits during silicic explosive eruptions

Aravena, Álvaro[1*]; de' Michieli Vitturi, Mattia[2]; Cioni, Raffaello[1]; Neri, Augusto[2].

1 Dipartimento di Scienze della Terra, Università di Firenze, 50121 Florence, Italy.

2 Istituto Nazionale di Geofisica e Vulcanologia, Sezione di Pisa, 56126 Pisa, Italy.

A. Conduit model: system of equations

MAMMA is an open-source 1D non-isothermal multiphase steady-state conduit model developed from the algorithm described by de' Michieli Vitturi et al. (2011), which has been largely employed for the study of explosive and effusive eruptions (e.g., La Spina et al., 2015; Aravena et al., 2017; Aravena et al., 2018). The model is capable of considering the main processes that magmas experience during ascent and is currently available online (http://demichie.github.io/MAMMA), where the documentation of the model is also present. The ascending magma is described as a mixture of two phases ($i = 1, 2$), whose natures depend on the relative position of the fragmentation level. Below the fragmentation level, phase 1 includes crystals, dissolved gas and melt (continuous phase); whereas phase 2 is composed by the exsolved gas bubbles (discontinuous phase). On the other hand, above magma fragmentation, phase 1 is composed by the dispersed magma fragments (discontinuous phase), while phase 2 corresponds to the continuous exsolved gas phase. The system of equations for this two-phase compressible flow was produced using the theory of thermodynamically compatible systems (Romenski et al., 2010), and it is formulated as an hyperbolic system of partial differential equations coupled with non-differential source terms (La Spina et al., 2015). The system of equations includes the conservation laws for total mass (Eq. 1), momentum (Eq. 2), energy (Eq. 3), mass of crystals (Eq. 4), mass of dissolved water (Eq. 5) and mass of exsolved water (Eq. 6), and additional equations for controlling the relative velocity between the phases (Eq. 7) and volume fraction of phase 1 (Eq. 8). It is worth noting that the terms related to the injected water appear in the conservation equations of total mass, mass of dissolved water and energy.

(1) $\frac{\partial}{\partial z}(\rho u \pi R^2) = 2\pi R J_{ex}$

(2) $$\frac{\partial}{\partial z}((\alpha_1\rho_1u_1^2+\alpha_1p_1+\alpha_2\rho_2u_2^2+\alpha_2p_2)\pi R^2)=-\rho g\pi R^2-8\pi\chi_1\mu u_1-\frac{\chi_2\lambda_w\rho_2u_2^2\pi R}{4}$$

(3) $$\frac{\partial}{\partial z}\left(\left(\alpha_1\rho_1u_1\left(e_1+\frac{p_1}{\rho_1}+\frac{u_1^2}{2}\right)+\alpha_2\rho_2u_2\left(e_2+\frac{p_2}{\rho_2}+\frac{u_2^2}{2}\right)-\rho x_1x_2(u_1-u_2)(s_1-s_2)T\right)\pi R^2\right)$$
$$=-\rho gu\pi R^2-8\pi\chi_1\mu u_1^2-\frac{\chi_2\lambda_w\rho_2u_2^3\pi R}{4}+2\pi RJ_{ex}c_wT_w$$

(4) $$\frac{\partial}{\partial z}(\alpha_1\rho_c\alpha_cu_1\pi R^2)=-\frac{1}{\tau^{(c)}}\alpha_1\rho_c(\alpha_c-\alpha_c^{eq})\pi R^2$$

(5) $$\frac{\partial}{\partial z}(x_d\alpha_1(\rho_1-\alpha_c\rho_c)u_1\pi R^2)=2\pi RJ_{ex}-\frac{1}{\tau^{(d)}}(x_d-x_d^{eq})\,\alpha_1(\rho_1-\alpha_c\rho_c)\pi R^2$$

(6) $$\frac{\partial}{\partial z}(\alpha_2\rho_2u_2\pi R^2)=\frac{1}{\tau^{(d)}}(x_d-x_d^{eq})\,\alpha_1(\rho_1-\alpha_c\rho_c)\pi R^2$$

(7) $$\frac{\partial}{\partial z}\left(\left(\frac{u_1^2}{2}-\frac{u_2^2}{2}+e_1-e_2+\frac{p_1}{\rho_1}-\frac{p_2}{\rho_2}-(s_1-s_2)T\right)\pi R^2\right)$$
$$=-\frac{8\pi\chi_1\mu u_1}{\alpha_1\rho_1}+\frac{\chi_2\lambda_wu_2^2\pi R}{4\alpha_2}-\frac{\rho}{\rho_1\rho_2}\delta_f(u_1-u_2)\pi R^2$$

(8) $$\frac{\partial}{\partial z}(\rho u\alpha_1\pi R^2)=-\frac{1}{\tau^{(p)}}(p_2-p_1)\pi R^2$$

where z is the vertical coordinate, ρ is mixture density, u is mixture velocity, R is conduit radius,, J_{ex} is the mass flux of external water (Eq. 9), α_i is volumetric fraction of phase i, ρ_i is density of phase i, u_i is velocity of phase i, p_i is pressure of phase i, g is the acceleration of gravity, χ_i controls the inclusion of the wall friction component (1 or 0, function of the continuous phase index), μ is mixture viscosity, λ_w is a drag factor (Degruyter et al., 2012), e_i is the internal energy of phase i, x_i is the mass fraction of phase i, s_i is the specific entropy of phase i, T is mixture temperature, c_w is the specific heat capacity of external water, T_w is external water temperature, ρ_c is crystals density, α_c is the volumetric fraction of crystals in phase 1, $\tau^{(c)}$ is the crystallization relaxation parameter, α_c^{eq} is the equilibrium value of α_c, x_d is the mass fraction of dissolved gas in the phase composed by melt

and dissolved water, $\tau^{(d)}$ is the characteristic time which controls gas exsolution, x_d^{eq} is the equilibrium value of x_d and δ_f is an additional drag factor.

It is worth to highlight the differences between the governing equations of this model and those adopted in Starostin et al. (2005). In both the models, the energy equation is solved considering the effect of the injection of external water on total energy. For this reason, the contribution should consider the total energy of the added water (i.e., $J_{ex}c_wT_w$) and not only the thermal energy in excess with respect to the magmatic mixture temperature, as done in Starostin et al. (2005). Following Starostin et al. (2005), for example, an inlet of water vapor at the same temperature of the magmatic mixture would not increase the total energy of the mixture. Thus, it seems to us that the term proposed in their work (q in Eq. 25, p. 140) would be correct for an equation for the temperature, but not when adopted in an equation representing the conservation of total energy. In addition, in the model of Starostin et al. (2005), when water infiltrates the conduit it vaporizes instantaneously, while in our model, where disequilibrium is allowed and modeled, it is possible to have a delay between injection of water and vaporization.

On the other hand, following Starostin et al. (2005), the injection of external water is modeled using the Darcy's law:

$$(9)\ J_{ex} = \begin{cases} \dfrac{\rho_w k}{\mu_w} \cdot \dfrac{p_a - p_1}{R} & \text{if } p_a \geq p_1 \\ 0 & \text{if } p_a < p_1 \end{cases}$$

where ρ_w is the external water density, k is aquifer permeability, μ_w is external water viscosity and p_a is aquifer pressure.

The steady-state solution is computed using a shooting technique, which is based on an iterative scheme for searching the initial magma ascent velocity (i.e., at the conduit bottom) that allows to produce atmospheric pressure or a choked flow at the exit of the conduit (de' Michieli Vitturi et al., 2008). In addition, the model requires the inclusion of some constitutive equations for modelling the magma behaviour: (1) magma rheology, (2) crystallization, (3) gas exsolution, (4)

outgassing processes and (5) equations of state (see Section B). The validity of the constitutive equations for simulations characterized by high mass fractions of external water has been also evaluated. Since these conditions are exclusively observed above the fragmentation level and considering the typical timespan at which magmas ascent under this condition, most of the adopted constitutive equations do not influence significantly the resulting eruptive dynamics (e.g., viscosity, solubility law, crystallization, outgassing). In particular, the adopted equations of state predict valid results of ρ_1 for mass fractions of injected water up to 40 wt. %. This fact is mainly controlled by the cooling effect of the external water. It is also worth noting that our formulation does not consider and model the small-scale processes that magma-water interaction involves (e.g., FCI, magma quenching, characteristic timespan for homogenization) and the aquifer response (e.g., changes in temperature and pressure fields, water migration) (Delaney, 1982). Still, this model indicates for the first time important constraints about the conditions needed to produce phreatomagmatic eruptions and the amount of water involved in these processes.

B. Conduit model: constitutive equations

In this work, we have performed a set of numerical simulations reproducing representative conditions of trachytic, dacitic and rhyolitic explosive volcanism, using variable input values for the following parameters: (1) inlet overpressure (from -10 MPa to +10 MPa respect to the lithostatic pressure), water content at conduit bottom (4.0-6.0 wt. % for trachytic magmas; 4.5-6.5 wt. % for dacitic and rhyolitic magmas), conduit radius (6-30 m for trachytic magmas, 10-35 m for dacitic magmas and 30-90 m for rhyolitic magmas), aquifer depth (500-2000 m) and aquifer thickness (150-300 m). The model also requires the inclusion of appropriate constitutive equations for modelling the magma behaviour, as described in this section.

B.1 Magma rheology model

Since it has been suggested a strong effect of crystals and exsolved gas bubbles on mixture rheology (Dingwell et al., 1993; Manga and Loewenberg, 2001), magma viscosity (μ) is calculated using:

$$\mu = \mu_{melt} \cdot \theta_c(\alpha_c) \cdot \theta_g(\alpha_g) \quad (10)$$

where μ_{melt} is the crystals and bubbles-free viscosity, whereas $\theta_c(\alpha_c)$ and $\theta_g(\alpha_g)$ account for the effect of crystals and bubbles on magma viscosity.

For determining μ_{melt}, we adopted different models for the different magma compositions considered in this work. For rhyolitic and dacitic magmas, we considered the models presented by Hess and Dingwell (1996) and Whittington et al. (2009), respectively. On the other hand, in order to describe a representative rheology for trachytic melts, we adopted the model described by Giordano et al. (2008), using geochemical data from Di Matteo et al. (2004). For calculating $\theta_c(\alpha_c)$, we adopted the following formulation (Costa, 2005):

(11) $\theta_c(\alpha_c) = [1 - F(\alpha_c, c_1, c_2, c_3)]^{c_4/c_1}$

(12) $F(\alpha_c, c_1, c_2, c_3) = c_1 \cdot \mathrm{erf}\left[\frac{\sqrt{\pi}}{2} \cdot \alpha_c \cdot \left(1 + \frac{c_2}{(1-\alpha_c)^{c_3}}\right)\right]$

where c_1, c_2, c_3 and c_4 are fitting parameters.

On the other hand, Eq. 13 describes the expression employed for calculating $\theta_g(\alpha_g)$ (Costa et al., 2007).

(13) $\theta_g(\alpha_g) = \frac{1}{1 + 25 \cdot Ca^2}\left(\frac{1}{1-\alpha_g} + 25 \cdot Ca^2 \cdot (1-\alpha_g)^{5/3}\right)$

where Ca is capillarity number, calculated following Llewellin and Manga (2005).

B.2 Solubility model

We adopted the Henry's law:

(14) $x_d^{eq} = \sigma \left(\frac{p_g}{1\ [\mathrm{Pa}]}\right)^{S_\epsilon}$

where p_g is pressure of the gas component, σ is the solubility coefficient and S_ϵ is the solubility exponent. The adopted solubility coefficients are derived from Zhang (1999), Moore et al. (1998) and Di Matteo et al. (2004) for rhyolitic, dacitic and trachytic magmas, respectively.

B.3 Crystallization model

We adopted the following crystallization model (de' Michieli Vitturi et al., 2010):

(15) $\alpha_c^{eq} = \min\left[\alpha_{c,max}, \alpha_{c,0} + 0.55 \cdot (0.58815 \cdot p^{-0.5226})\right]$

where $\alpha_{c,max}$ is the maximum crystallinity and $\alpha_{c,0}$ is the initial volume fraction of crystals.

B.4 Outgassing model

For calculating $|dp/dz|$, we use a definition by parts (Degruyter et al., 2012):

$$(16)\quad \left|\frac{dp}{dz}\right| = \begin{cases} \dfrac{\mu_g(\Delta u)}{k_D} + \dfrac{\rho_g(\Delta u)^2}{k_I} & \text{if } \alpha_g \le \alpha_{cr} \\ \left(\dfrac{\mu_g(\Delta u)}{k_D} + \dfrac{\rho_g(\Delta u)^2}{k_I}\right)^{1-t} \left(\dfrac{3C_D\rho_g(\Delta u)^2}{8r_a}\right)^{t} & \text{if } \alpha_{cr} < \alpha_g < \alpha_t \\ \dfrac{3C_D\rho_g(\Delta u)^2}{8r_a} & \text{if } \alpha_g \ge \alpha_t \end{cases}$$

where Δu is the velocity difference between both phases, subscript g refers to the exsolved gas phase, C_D is a drag coefficient, r_a is the average size of the fragmented magma particles, $t = (\alpha_g - \alpha_{cr})/(\alpha_t - \alpha_{cr})$, α_t controls the range of the transitional domain, while k_D and k_I are the Darcian and inertial permeabilities, respectively (Eqs. 17 and 18). Please note that $|dp/dz| = \delta_f \cdot \Delta u$.

$$(17)\quad k_D = \frac{(f_{rb}r_b)^2}{8}\alpha_g^m$$

$$(18)\quad k_I = \frac{f_{rb}r_b}{f}\alpha_g^{(1+3m)/2}$$

$$(19)\quad r_b = \left(\frac{\alpha_g}{\frac{4\pi}{3}N_{bd}\alpha_l}\right)^{1/3}$$

where f_{rb} is the throat-bubble size ratio, r_b is the average bubble size, N_{bd} is the bubble density number, while f and m are fitting parameters.

B.5 Equations of state

For defining the specific internal energy, pressure and specific entropy of melt, crystals and dissolved water, a linearized version of the Mie-Grüneisen equations of state was adopted (Le Métayer et al., 2005):

$$(20)\ e_k(\rho_k, T) = \bar{e}_k + c_{v,k}T + \frac{\rho_{0,k}C_{0,k}^2 - \gamma_k p_{0,k}}{\gamma_k \rho_k}$$

$$(21)\ s_k(\rho_k, T) = s_{0,k} + c_{v,k} \cdot \ln\left(\frac{T}{T_{0,k}}\left(\frac{\rho_{0,k}}{\rho_k}\right)^{\gamma_k - 1}\right)$$

where $\bar{e}_k$ represents the formation energy, $c_{v,k}$ is the specific heat capacity at constant volume, $\rho_{0,k}$ and $C_{0,k}$ are the density and sound speed at a reference state, γ_k is the adiabatic exponent, $p_{0,k}$ and $s_{0,k}$ are the pressure specific entropy at a reference state and $T_{0,k}$ is temperature at the reference state. Subscript k refers to the melt, dissolved water or crystals.

For the exsolved water, we adopted the ideal gas model:

$$(22)\ e_g(\rho_g, T) = c_{v,g}T + \bar{e}_g$$

$$(23)\ s_g(\rho_g, T) = c_{v,g} \cdot \ln\left(\frac{T}{T_{0,g}}\left(\frac{\rho_{0,g}}{\rho_g}\right)^{\gamma_g - 1}\right)$$

C. Supplementary Figures

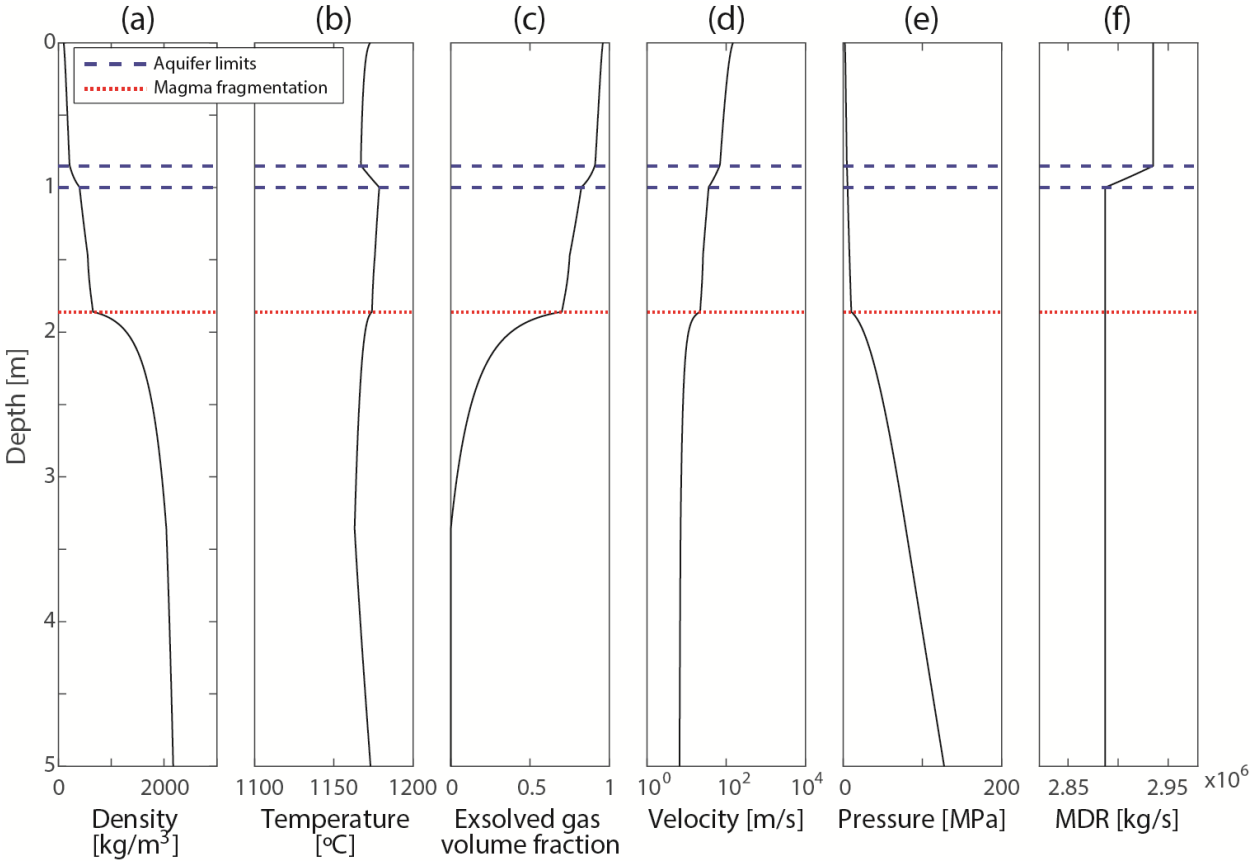

Figure DR1. Profiles along the conduit of some physical variables, for a specific simulation (trachytic magma, water content at conduit bottom: 4.0 wt. %, inlet overpressure: 0 MPa, conduit radius: 8 m, aquifer permeability: 10^{-12} m^2, aquifer depth: 850 – 1000 m, geopressured aquifer). It represents a typical case of simulations with the aquifer located above the fragmentation level. A: Density. B: Temperature. C: Exsolved gas volume fraction. D: Velocity. E: Pressure. F: Mass discharge rate.

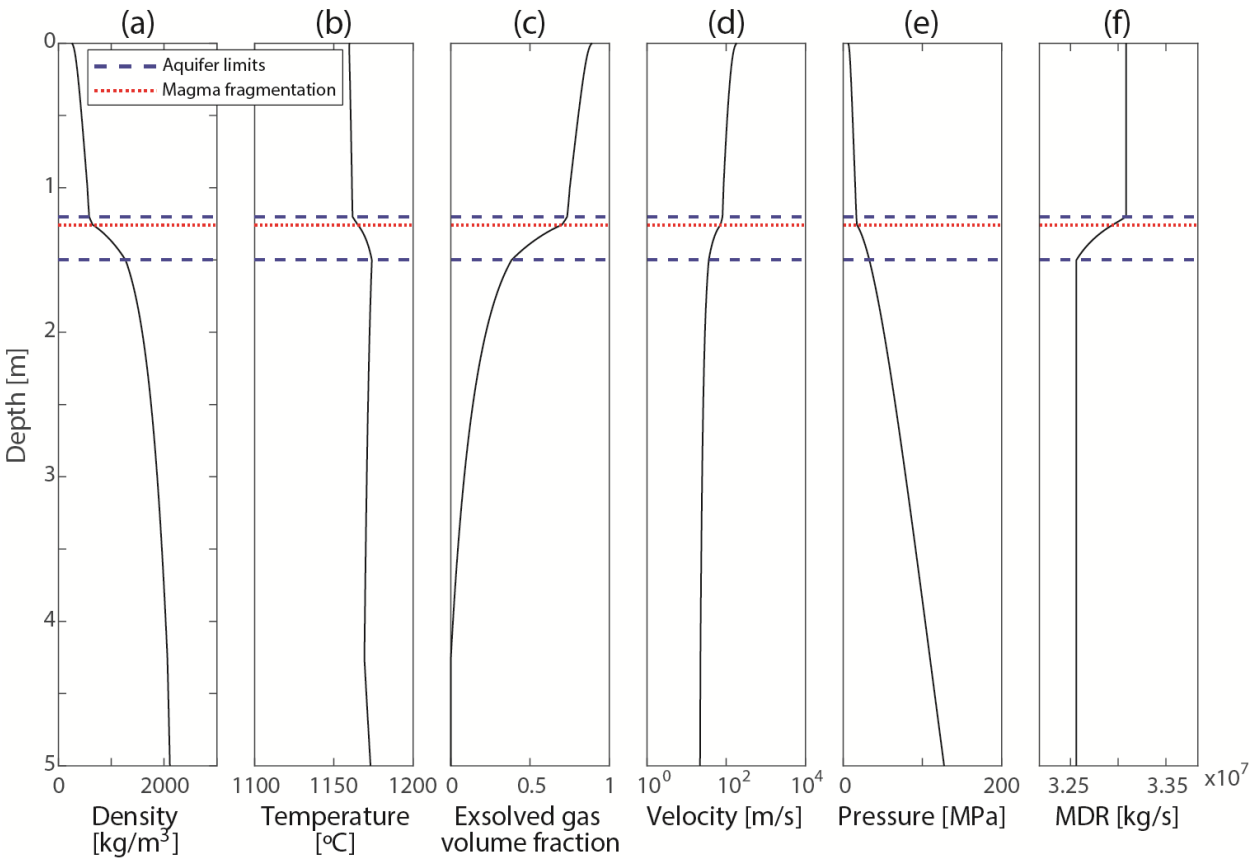

Figure DR2. Profiles along the conduit of some physical variables, for a specific simulation (trachytic magma, water content at conduit bottom: 5.0 wt. %, inlet overpressure: 0 MPa, conduit radius: 15 m, aquifer permeability: 10^{-11} m^2, aquifer depth: 1200 – 1500 m, geopressured aquifer). It is a representative case of simulations where aquifer position coincides with fragmentation level. A: Density. B: Temperature. C: Exsolved gas volume fraction. D: Velocity. E: Pressure. F: Mass discharge rate.

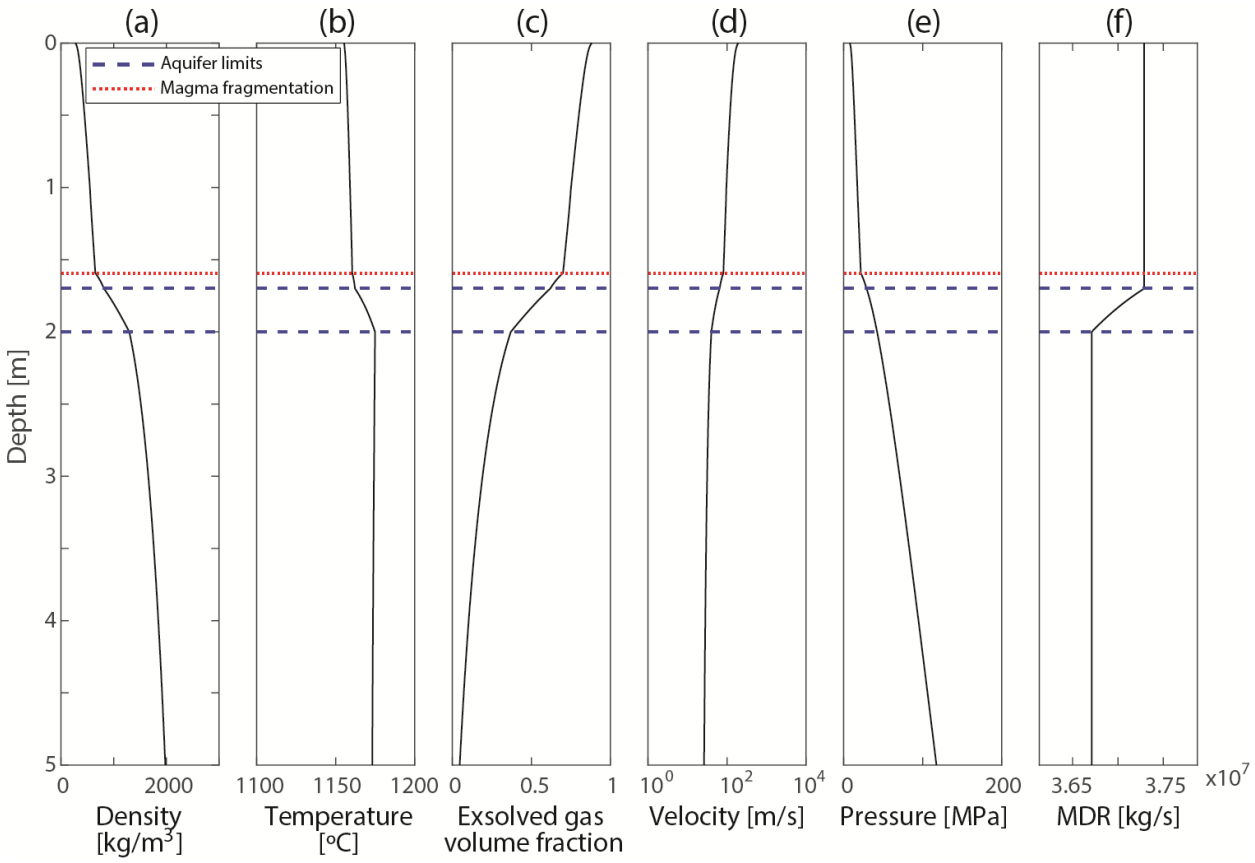

Figure DR3. Profiles along the conduit of some physical variables, for a specific simulation (trachytic magma, water content at conduit bottom: 6.0 wt. %, inlet overpressure: -10 MPa, conduit radius: 15 m, aquifer permeability: 10^{-11} m^2, aquifer depth: 1700 - 2000 m, geopressured aquifer). It represents a typical case of simulations with the aquifer located below the fragmentation level. A: Density. B: Temperature. C: Exsolved gas volume fraction. D: Velocity. E: Pressure. F: Mass discharge rate.

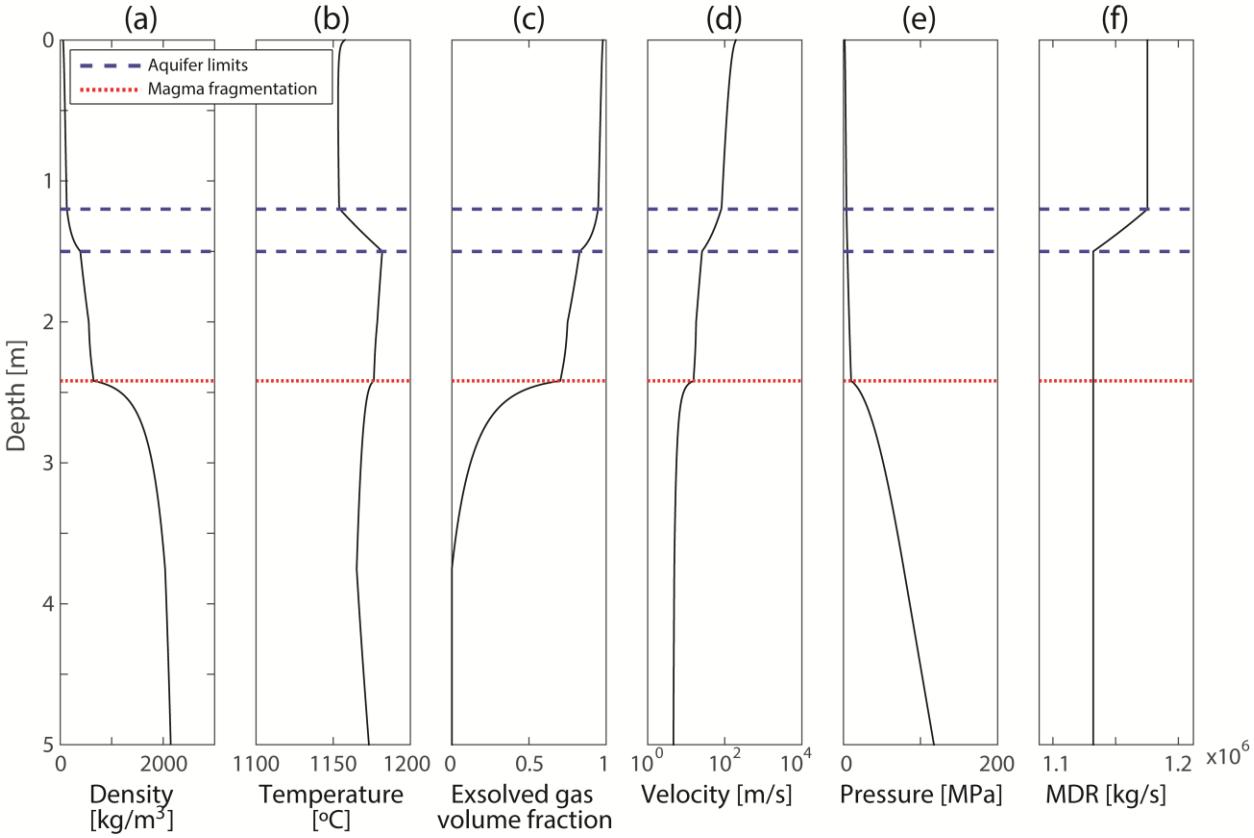

Figure DR4. Profiles along the conduit of some physical variables, for a specific simulation (trachytic magma, water content at conduit bottom: 4.0 wt. %, inlet overpressure: -10 MPa, conduit radius: 6 m, aquifer permeability: 10^{-12} m^2, aquifer depth: 1200 – 1500 m, normally pressured aquifer). It represents a typical case of simulations with the aquifer located above the fragmentation level. A: Density. B: Temperature. C: Exsolved gas volume fraction. D: Velocity. E: Pressure. F: Mass discharge rate.

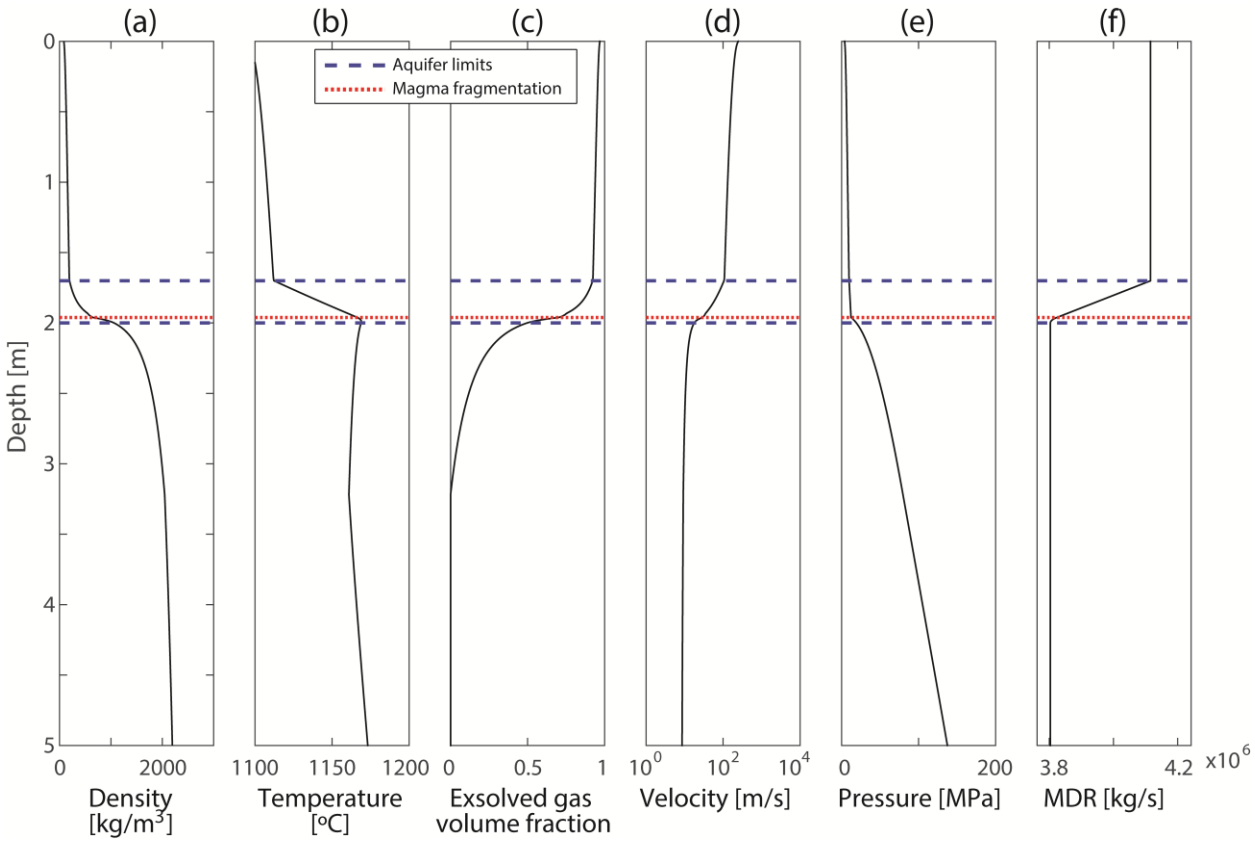

Figure DR5. Profiles along the conduit of some physical variables, for a specific simulation (trachytic magma, water content at conduit bottom: 4.0 wt. %, inlet overpressure: +10 MPa, conduit radius: 8 m, aquifer permeability: 10^{-11} m^2, aquifer depth: 1700 – 2000 m, normally pressured aquifer). It is a representative case of simulations where aquifer position coincides with fragmentation level. A: Density. B: Temperature. C: Exsolved gas volume fraction. D: Velocity. E: Pressure. F: Mass discharge rate.

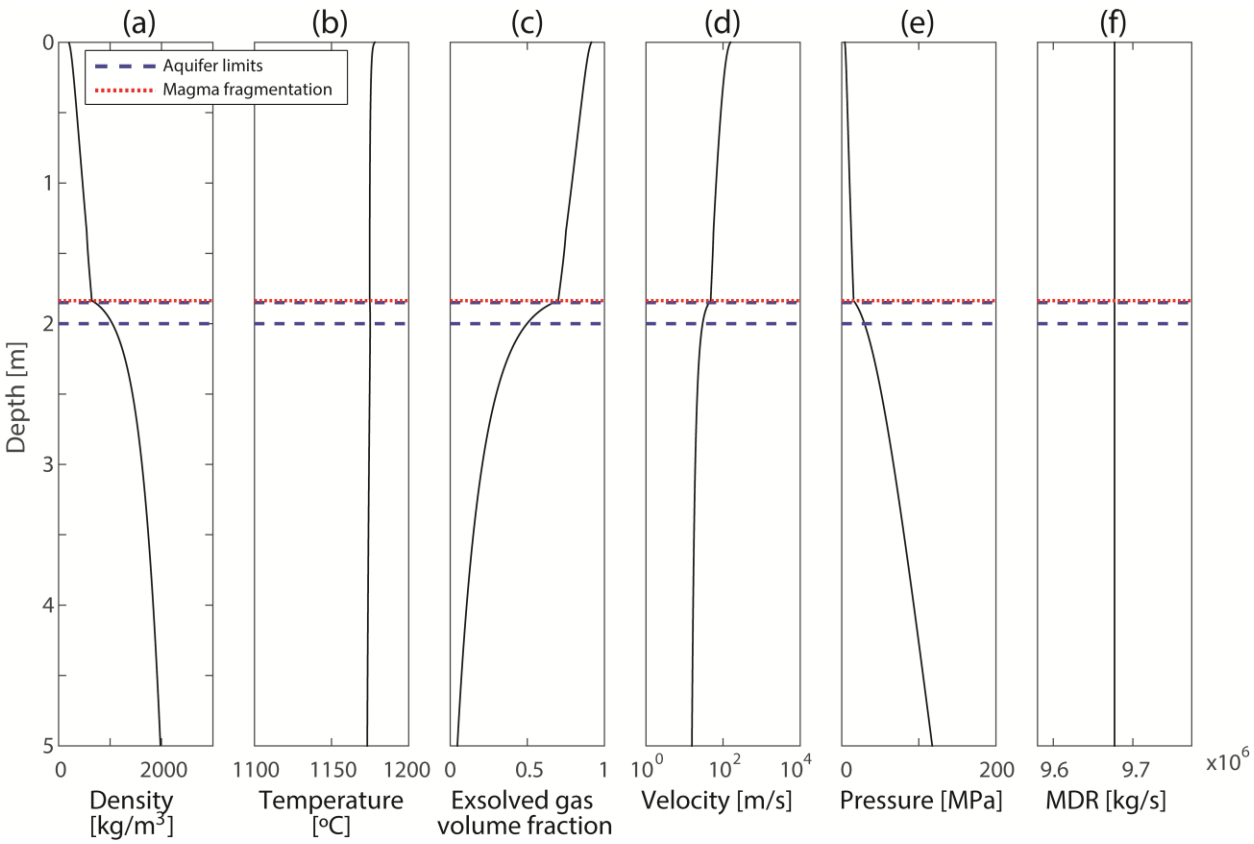

Figure DR6. Profiles along the conduit of some physical variables, for a specific simulation (trachytic magma, water content at conduit bottom: 6.0 wt. %, inlet overpressure: -10 MPa, conduit radius: 10 m, aquifer permeability: 10^{-11} m^2, aquifer depth: 1850 - 2000 m, normally pressured aquifer). It represents a typical case of simulations with the aquifer located below the fragmentation level. A: Density. B: Temperature. C: Exsolved gas volume fraction. D: Velocity. E: Pressure. F: Mass discharge rate.

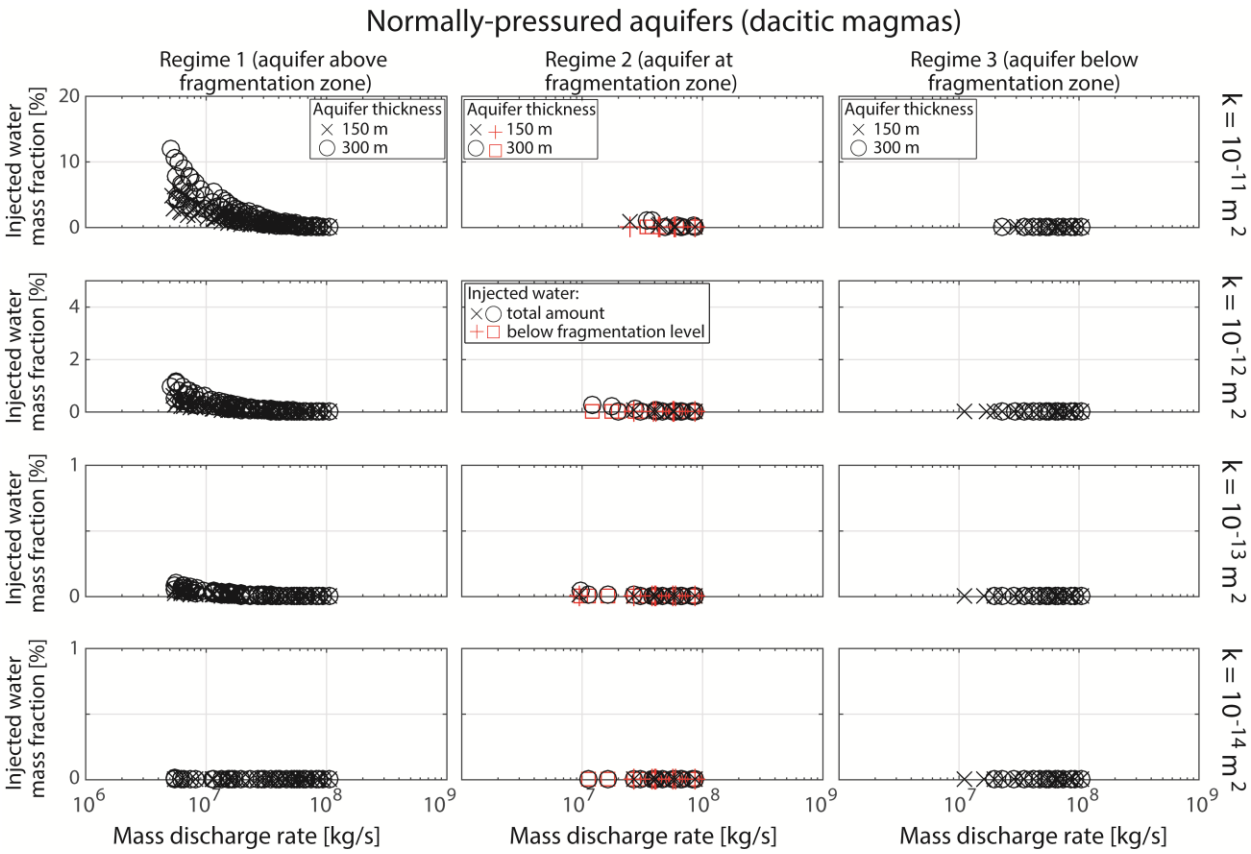

Figure DR7. Injected water mass fraction versus mass discharge rate, as a function of aquifer permeability (indicated in the right-hand side) and the relative position between the aquifer and magma fragmentation, considering normally pressured aquifers and dacitic magmas.

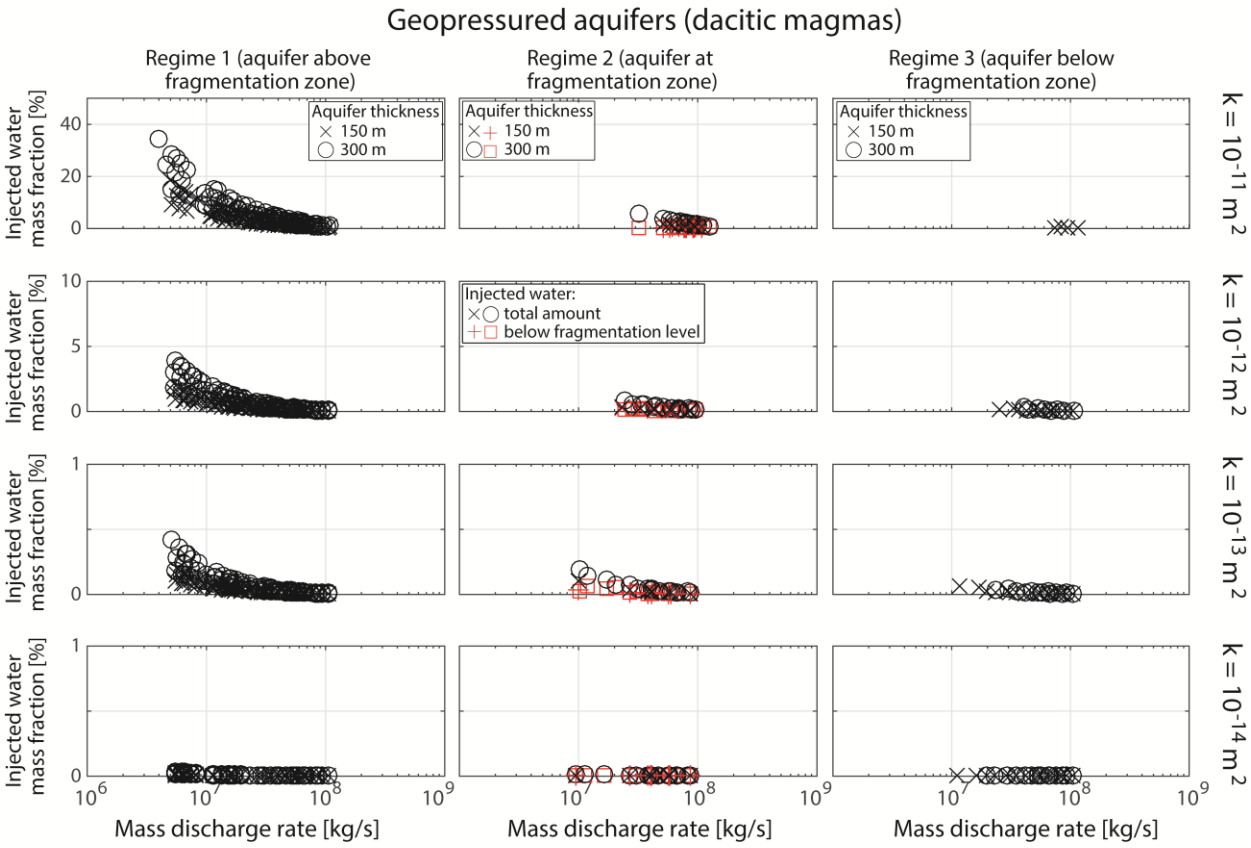

Figure DR8. Injected water mass fraction versus mass discharge rate, as a function of aquifer permeability (indicated in the right-hand side) and the relative position between the aquifer and magma fragmentation, considering geopressured aquifers and dacitic magmas.

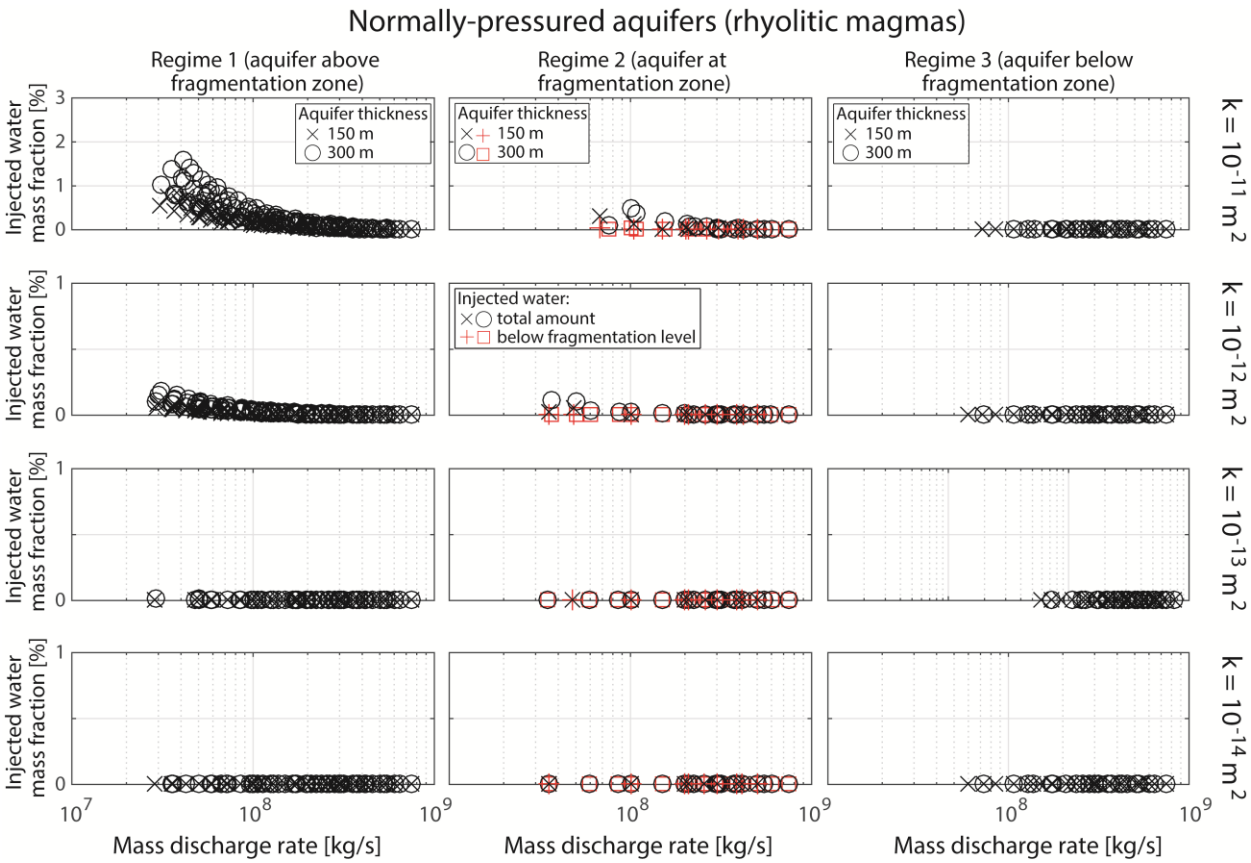

Figure DR9. Injected water mass fraction versus mass discharge rate, as a function of aquifer permeability (indicated in the right-hand side) and the relative position between the aquifer and magma fragmentation, considering normally pressured aquifers and rhyolitic magmas.

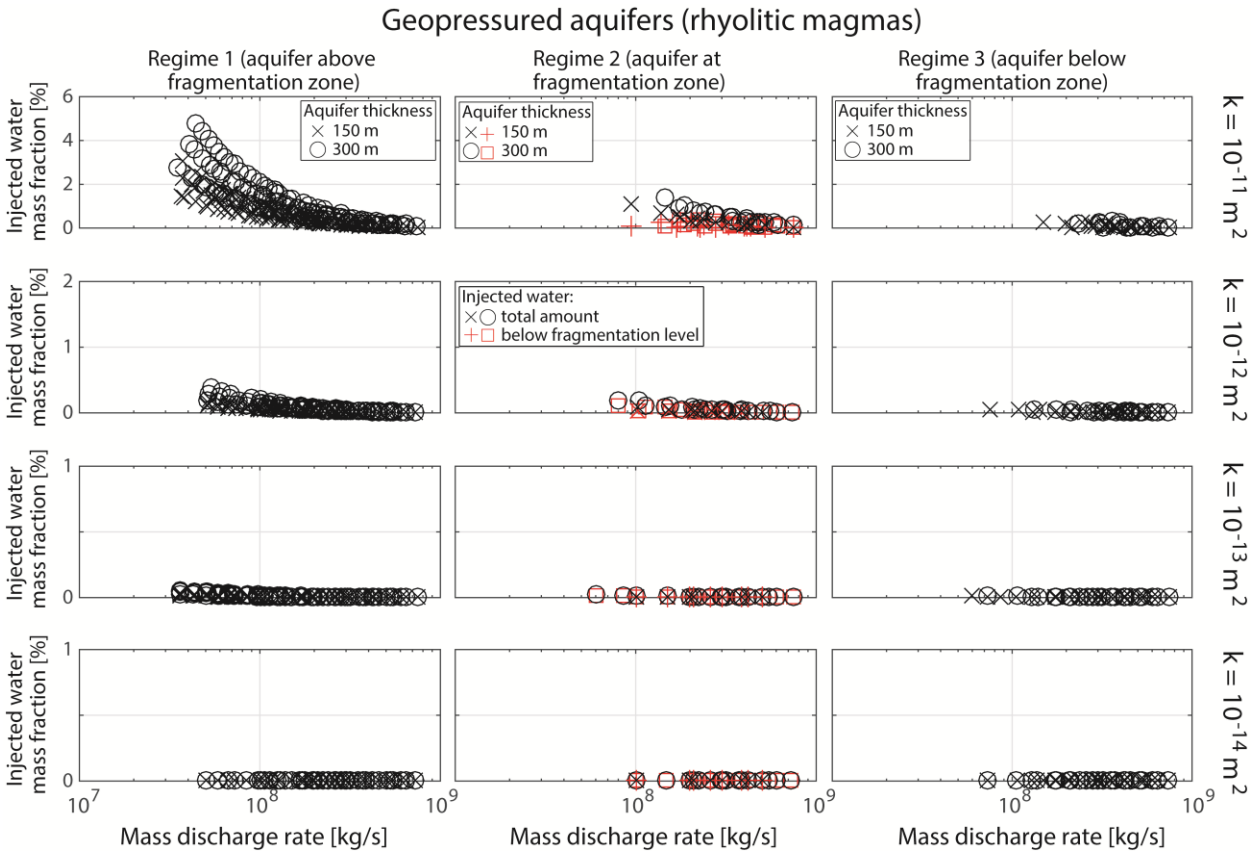

Figure DR10. Injected water mass fraction versus mass discharge rate, as a function of aquifer permeability (indicated in the right-hand side) and the relative position between the aquifer and magma fragmentation, considering geopressured aquifers and rhyolitic magmas.

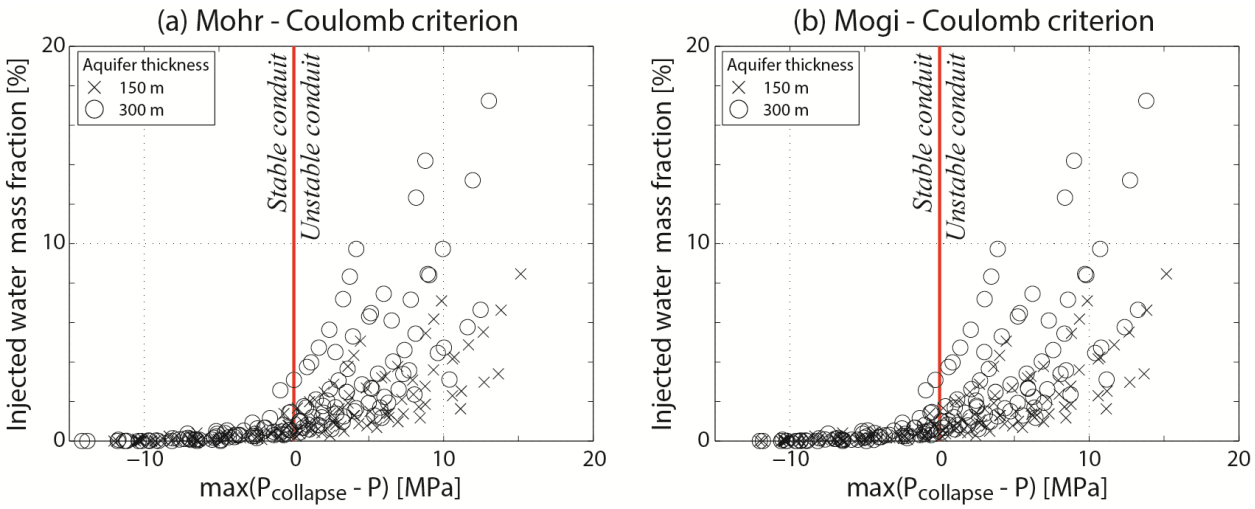

Figure DR11. Injected water mass fraction versus instability index, using Mohr – Coulomb (a) and Mogi – Coulomb (b) collapse criteria. We present here the results related to a set of simulations with variable values for inlet overpressure (from -10 MPa to +10 MPa), conduit radius (6 – 30 m) and water content (4.0 – 6.0 wt. %), considering normally-pressured and geopressured aquifers. For clarity, we only include simulations of trachytic magmas with aquifer permeability of 10^{-12} m^2. In order to quantify the instability degree of the conduit, we used the 'instability index' defined as $\max(P_{collapse}(z) - P(z))$ (Aravena et al., 2017), where $P_{collapse}(z)$ is the minimum pressure needed to avoid conduit collapse according to Mohr - Coulomb and Mogi - Coulomb stability criteria (Al-Ajmi and Zimmerman, 2006), and $P(z)$ is the pressure profile along the conduit, computed from numerical modelling. The values employed for country rock mechanical parameters are thought to be representative of natural conditions and are shown in Table DR1.

D. Supplementary Tables

Table DR1. Mechanical parameters employed in the analysis of conduit stability, representative of typical conditions of country rocks (Hoek and Brown, 1997).

Parameter	Value
Rock cohesion	5 MPa
Angle of friction	38º
Vertical stress gradient	26 kPa/m
Both horizontal stress gradients	18 kPa/m

E. References of supplementary material

Al-Ajmi, A. M., and Zimmerman, R. W., 2006, Stability analysis of vertical boreholes using the Mogi–Coulomb failure criterion: International Journal of Rock Mechanics and Mining Sciences, v. 43, no. 8, p. 1200-1211.

Aravena, A., de' Michieli Vitturi, M., Cioni, R., and Neri, A., 2017, Stability of volcanic conduits during explosive eruptions: Journal of Volcanology and Geothermal Research, v. 339, p. 52-62.

Aravena, A., Cioni, R., de' Michieli Vitturi, M., and Neri, A., 2018, Conduit stability effects on intensity and steadiness of explosive eruptions: Scientific Reports, v. 8, no. 4125.

Costa, A., 2005, Viscosity of high crystal content melts: dependence on solid fraction: Geophysical Research Letters, v. 32, no. 22.

Costa, A., Melnik, O., and Sparks, R., 2007, Controls of conduit geometry and wallrock elasticity on lava dome eruptions: Earth and Planetary Science Letters, v. 260, no. 1, p. 137-151.

de' Michieli Vitturi, M., Clarke, A., Neri, A., and Voight, B., 2008, Effects of conduit geometry on magma ascent dynamics in dome-forming eruptions: Earth and Planetary Science Letters, v. 272, no. 3, p. 567-578.

de' Michieli Vitturi, M., Clarke, A., Neri, A., and Voight, B., 2010, Transient effects of magma ascent dynamics along a geometrically variable dome-feeding conduit: Earth and Planetary Science Letters, v. 295, no. 3, p. 541-553.

de' Michieli Vitturi, M., Clarke, A., Neri, A., and Voight, B., 2011, Assessing the influence of disequilibrium crystallization and degassing during magma ascent in effusive and explosive eruptions, in Proceedings AGU Fall Meeting Abstracts 2011, v. 1, p. 05.

Degruyter, W., Bachmann, O., Burgisser, A., and Manga, M., 2012, The effects of outgassing on the transition between effusive and explosive silicic eruptions: Earth and Planetary Science Letters, v. 349, p. 161-170.

Delaney, P. T., 1982, Rapid intrusion of magma into wet rock: groundwater flow due to pore pressure increases: Journal of Geophysical Research: Solid Earth, v. 87, no. B9, p. 7739-7756.

Di Matteo, V., Carroll, M., Behrens, H., Vetere, F., and Brooker, R., 2004, Water solubility in trachytic melts: Chemical Geology, v. 213, no. 1, p. 187-196.

Dingwell, D. B., Bagdassarov, N., Bussod, G., and Webb, S. L., 1993, Magma rheology, in: Miner. Assoc. Canada Short Course Handbook on Experiments at High Pressures and Application to the Earth's Mantle, v. 21, 1993, pp. 131-196.

Giordano, D., Russell, J. K., and Dingwell, D. B., 2008, Viscosity of magmatic liquids: a model: Earth and Planetary Science Letters, v. 271, no. 1, p. 123-134.

Hess, K., and Dingwell, D., 1996, Viscosities of hydrous leucogranitic melts: A non-Arrhenian model: American Mineralogist, v. 81, no. 9-10, p. 1297-1300.

Hoek, E., and Brown, E., 1997, Practical estimates of rock mass strength: International Journal of Rock Mechanics and Mining Sciences, v. 34, no. 8, p. 1165-1186.

La Spina, G., Burton, M., and de' Michieli Vitturi, M., 2015, Temperature evolution during magma ascent in basaltic effusive eruptions: A numerical application to Stromboli volcano: Earth and Planetary Science Letters, v. 426, p. 89-100.

Le Métayer, O., Massoni, J., and Saurel, R., 2005, Modelling evaporation fronts with reactive Riemann solvers: Journal of Computational Physics, v. 205, no. 2, p. 567-610.

Llewellin, E., and Manga, M., 2005, Bubble suspension rheology and implications for conduit flow: Journal of Volcanology and Geothermal Research, v. 143, no. 1, p. 205-217.

Manga, M., and Loewenberg, M., 2001, Viscosity of magmas containing highly deformable bubbles: Journal of Volcanology and Geothermal Research, v. 105, no. 1, p. 19-24.

Moore, G., Vennemann, T., and Carmichael, I., 1998, An empirical model for the solubility of H2O in magmas to 3 kilobars: American Mineralogist, v. 83, no. 1, p. 36-42.

Romenski, E., Drikakis, D., and Toro, E., 2010, Conservative models and numerical methods for compressible two-phase flow: Journal of Scientific Computing, v. 42, no. 1, p. 68-95.

Starostin, A., Barmin, A., and Melnik, O., 2005, A transient model for explosive and phreatomagmatic eruptions: Journal of Volcanology and Geothermal Research, v. 143, no. 1, p. 133-151.

Whittington, A. G., Hellwig, B. M., Behrens, H., Joachim, B., Stechern, A., and Vetere, F., 2009, The viscosity of hydrous dacitic liquids: implications for the rheology of evolving silicic magmas: Bulletin of Volcanology, v. 71, no. 2, p. 185-199.

Zhang, Y., 1999, H2O in rhyolitic glasses and melts: measurement, speciation, solubility, and diffusion: Reviews of Geophysics, v. 37, no. 4, p. 493-516.